Letter to the Editor

Stimulated Ag Nanoparticles by Pulsed Laser Ablation for Breast Cancer Treatment*

WAN MOHD SHUKRI Wan Norsyuhada[1], BAKHTIAR Hazri[1], ISLAM Shumaila[1,#], BIDIN Noriah[1], BABA Sayang[2], HAMDAN Salehhuddin[2], and CHE ABDULLAH Mohd Azahar[3]

Currently, breast cancer is the most common new cancer diagnosis and is a leading cause of mortality among women in developing and under-developing countries. Hence, several techniques, such as radiation therapy, chemotherapy, and surgery, have been used to treat breast cancer. However, the use of metallic nanoparticles (NPs) in photothermal therapy is attracting considerable attention as they allow high heat deposition in tumor cells with low-power lasers and thus minimizes the damage around healthy tissues from localized hyperthermia[1]. Researchers have mostly used infrared lasers rather than breast cancer cells for photothermal therapy[2,3]. Moreover, photothermal therapy using a pulsed Q-switched neodymium-doped yttrium aluminum garnet (Nd:YAG) laser with hyperthermic effects in breast cancer cells (MDA-MB-468) has rarely been reported. Therefore, this work focused on silver NPs (AgNPs) stimulated by 0.52 J/mm^2 with a 532-nm Q-switched Nd:YAG pulsed laser for breast cancer cell treatment *in vitro*.

An Ag plate (99.99% pure) was immersed at the bottom of a cuvette and filled with 6 mL deionized water. A 1064-nm Q-switched Nd:YAG with a fluence of 0.057 J/mm^2 was applied with a pulse duration of 8 ns and a repetition rate of 6 Hz. The deionized water turned yellow after 5 min of laser ablation.

The absorption spectra of AgNPs were measured using a USB4000 spectrometer (Eastwest SVC, Singapore). The morphology and elemental composition of AgNPs were analyzed by transmission electron microscopy (TEM, HT7700; Hitachi, Tokyo, Japan) and high-resolution TEM (HRTEM, JEM-ARM200F; JEOL, Tokyo, Japan). Energy-dispersive X-ray (EDX) spectrometry, Fourier-transform infrared spectroscopy (FTIR) with attenuated total reflection (ATR) (L160000A; PerkinElmer, Waltham, MA), X-Ray diffractometry (SmartLab; Rigaku, Tokyo, Japan), and a Zetasizer Nano ZSP (Malvern Panalytical, Malvern, UK) confirmed the presence of elemental Ag, crystallinity, chemical bonding, and stability of AgNPs, respectively.

The human breast cancer cell line (MDA-MB-468, ATCC® HTB-132™) and the non-breast cancer (normal) cell line [WRL-68, ATCC® CL-48™ (HeLa derivative)] used in this study were purchased from American Type Culture Collection (Manassas, VA). Cells were cultured in complete growth medium [1% (v/v) penicillin/streptomycin (10,000 U/mL each), 2% (v/v) 2 mmol/L L-glutamine, and 10% (v/v) fetal bovine serum (FBS)]. After reaching 80%–90% confluency, 1 × 10^5 cells/mL cells were successfully seeded in 24-well plates and incubated at 37 °C with 5% CO_2. After a 24-h incubation, cells were treated with AgNPs [1.56%–6.25% volume (15.6–62.5 μg/mL)]. A Q-switched Nd:YAG laser (532 nm) was employed with a pulse duration of 8 ns and a repetition rate of 1 Hz. During cell treatment, a laser fluence of 0.104 J/mm^2 (5 times the number of pulses) for each AgNP concentration.

The influence of AgNPs on the viability of WRL-68 cells and MDA-MD-468 cells was assessed *via* an MTT cytotoxicity assay. Statistical analysis was performed using analysis of variance (ANOVA) with significance established at $P < 0.05$ compared to the control group.

Each well of a 24-well plate was seeded with 1 × 10^5 cells/mL of MDA-MD-468 cells and incubated for 24 h at 37 °C with 5% CO_2. AgNP-treated cells were laser-irradiated for 24 h and incubated for 72 h. Then, cells were scraped and pelleted at 2,000 g for 5 min. After that, the cells were incubated for 30 min

doi: 10.3967/bes2021.017

*This research was supported by the grant of Government of Malaysia: the Universiti Teknologi Malaysia [R.J130000.3509.06G82, Q.J130000.3509.06G81].

1. Laser Centre, Institute IbnuSina for Scientific and Industrial Research, Universiti Teknologi Malaysia; 2. Faculty of Biosciences and Medical Engineering, Universiti Teknologi Malaysia; 3. Faculty of Electrical Engineering, Universiti Teknologi Malaysia

at room temperature in dark conditions and observed using an inverted fluorescent microscope (T*i* Eclipse; Nikon, Tokyo, Japan).

Figure 1A shows a strong absorption peak of AgNPs at 400 nm, synthesized by pulsed laser ablation in liquid (PLAL) in deionized water, at a wavelength of 1,064 nm. After 5 min of ablation, the colloidal system changed from colorless (deionized water) to yellow (AgNPs) [Figure 1A inset (i)]. The spherical shape of AgNPs was confirmed by TEM (Figure 1B), which is in agreement with the literature[4]. In contrast, the histogram (Figure 1C) indicates an average particle size of 12 ± 6 nm with a narrow distribution. Furthermore, Figure 1D shows the crystallinity and different lattice arrangements, including Ag (200) with 0.28-nm lattice d-spacing, as noted in the literature[5].

Figure 2(A) shows the EDX spectrum of AgNPs from TEM images. Elemental weight distributions by percentage are tabulated in Figure 2A. The presence of Cu and C peaks are probably due to the C-coated Cu grid used for TEM and HRTEM analysis, as reported by other researchers[6]. Moreover, 55.3% of Ag along with the O peak confirms the presence of AgNPs in the colloidal system. Figure 2B shows the XRD graph of AgNPs. The graph exhibits 4 distinct diffraction peaks at 2θ values of 38.50°, 44.90°, 65.90°, and 77.30°, corresponding to the (111), (200), (220), and (311) planes of face-centered cubic Ag, in agreement with the literature[7]. Figure 2C shows the FTIR spectrum of AgNPs. The broad band at 3,302 cm^{-1} is associated with the stretching/vibration of –OH bonds. The peaks at 698 cm^{-1}, 1,223 cm^{-1}, 1,636 cm^{-1}, and 2,124 cm^{-1} are attributed to AgNPs, as documented in the literature[8], whereas the low-intensity peak at 1,386 cm^{-1} is assigned to the stretching/vibrations of the C-O bond. The zeta potential of synthesized AgNPs was observed as a sharp peak at −37.4 mV, suggesting a stable colloidal system (Figure 2D). It is implied that the surfaces of NPs are negatively charged and dispersed in the medium, as observed by other researchers[9]. The high negative value affirms the presence of repulsive forces between the

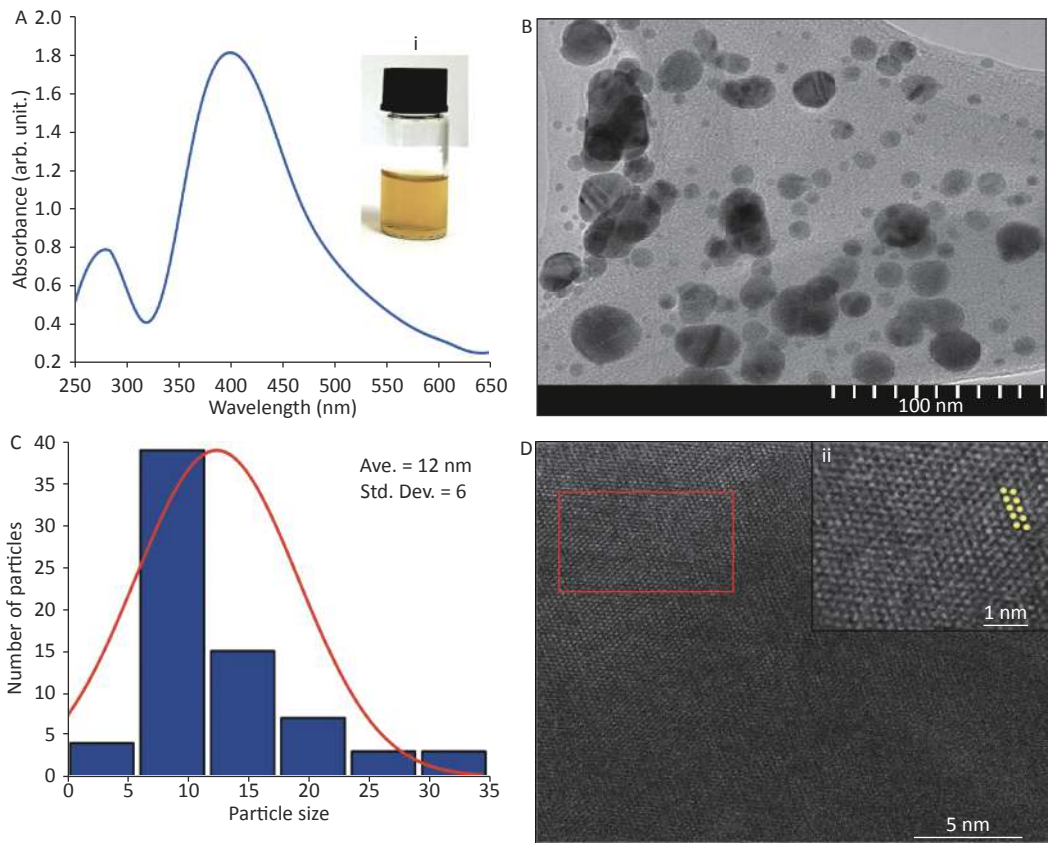

Figure 1. (A) Absorption spectrum of Ag nanoparticles (NPs); inset (i) corresponds to digital photograph of AgNP colloids after ablation. (B) Transmission electron microscopy (TEM) image. (C) Size distribution of AgNPs. (D) High-resolution TEM image and (ii) magnified image of marked area in (D).

particles, which proves that the particles are highly stable.

In order to observe the influence of AgNPs on MDA-MB-468 cells in photothermal therapy *in vitro* by an MTT assay, MDA-MB-468 cells were divided into three groups: (1) a control group (untreated cells), (2) treated with AgNPs without laser stimulation, and (3) 532-nm Q-switched Nd:YAG laser-stimulated AgNP-treated cells. Prior to the treatment, AgNPs at 0%–50% concentration were applied to WRL-68 cells with and without laser treatment (Figure 3I) to confirm the non-toxic effect. After a 72-h incubation, the viability of WRL-68 cells treated AgNPs (at 1.56%–6.25% concentration) without and with laser treatment showed non-toxic effects on cells (from 98.39% to 84.11% and from 96.02% to 64.28%, respectively). Then, the non-toxic dose (1.56%–6.25%) of AgNPs was applied to MDA-MB-468 cells with and without laser treatment for 72 h, and cell viability was calculated via the MTT assay. Figure 3II shows the low cell viability (from 80.96% to 28.10%) of MDA-MB-468 cells treated by AgNPs without laser treatment as compared to that of WRL-68 cells (from 98.39% to 84.11%). Moreover, after laser treatment, the viability of AgNP-treated MDA-MB-468 cells was more strongly reduced (from 74.86% to 15.11%) compared to that of WRL-68 cells (from 96.02% to 64.28%) (Figure 3III). In addition, MDA-MB-468 cells were more destroyed after laser treatment (from 74.86% to 15.11%) compared to before laser treatment (from 80.96% to 28.10%) with AgNPs at 1.56%–6.25% concentration (Figure 3II, 3III). Boca et al.[2] reported that continuous-wave (CW) laser-stimulated AgNPs within a 41–47 °C temperature range led to hyperthermic effects in photothermal therapy, resulting in breast cancer cell destruction. In contrast, the 532-nm Q-switched Nd:YAG pulsed laser-stimulated AgNP (6.25% concentration)-treated MDA-MB-468 cells showed 15.11% cell viability at 37 °C compared to 64.28% in WRL-68 cells. Furthermore, the Q-switched Nd:YAG pulsed laser can operate at a higher fluence and can control energy with the number of pulses as compared to a CW laser. The temperature of cells in the medium was measured as a function of 0.52 J/mm^2 energy fluence (5 × number of pulses) of a 532-nm pulsed laser by Equation 1:

$$Q = m_g c_g \Delta T \quad (1)$$

where m_g and c_g are the mass and heat capacity of glucose (medium of cells), respectively; ΔT is the difference in the median temperature. The reduction

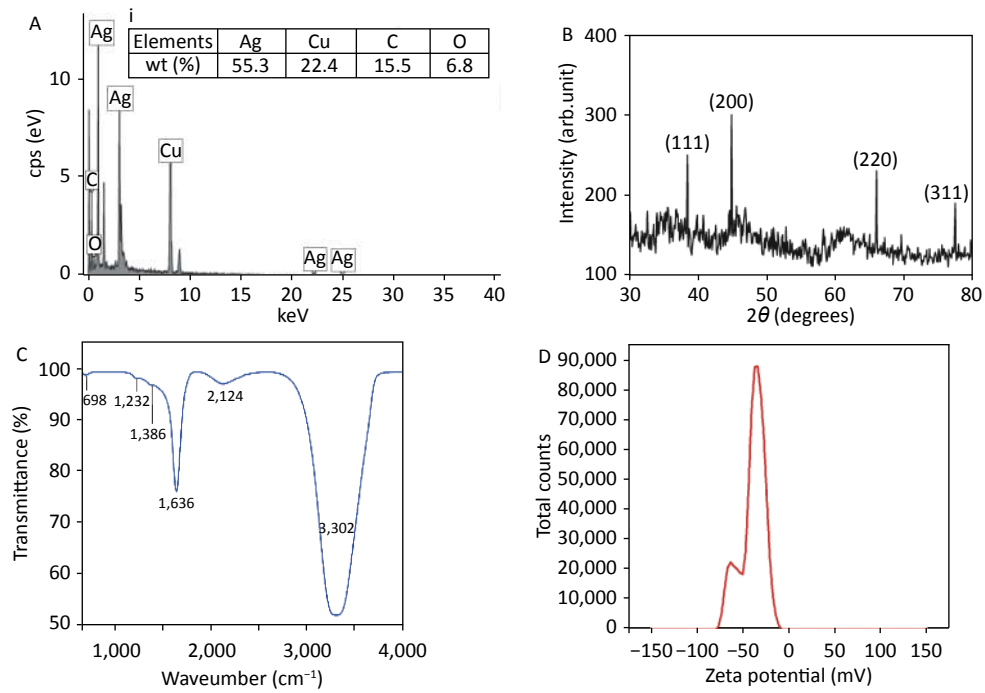

Figure 2. (A) Energy-dispersive X-ray spectrum of Ag nanoparticles (NPs) and inset (i) corresponding to elemental composition (% weight), (B) X-ray diffraction pattern of AgNPs, (C) Fourier-transform infrared spectrum of AgNPs, and (D) zeta potential distribution of AgNPs.

in viability of MDA-MB-468 cells after treatment with Q-switched Nd:YAG pulsed laser-stimulated AgNPs proves that synthesized AgNPs are an efficient anticancer agent. Furthermore, the behavior and response of synthesized AgNPs as an anticancer agent is in agreement with cisplatin, a standard anticancer agent[10].

The morphology of WRL-68 Figure 3A–C) and MDA-MD-468 (Figure 3a–c) cells treated with AgNPs with and without laser stimulation was observed by an inverted microscope after a 72-h incubation. WRL-68 cells treated with AgNPs without laser treatment (Figure 3B) and after laser treatment (Figure 3C) did not show any significant changes compared to untreated cells Figure 3A). However, MDA-MD-468 cells treated with AgNPs without laser treatment (Figure 3b) and with laser treatment (Figure 3c) show pseudo-spherical morphology, detachment, and loss of cell extensions compared to untreated cells (Figure 3a). The arrows Figure 3b, c) indicate changes in cell morphology after AgNP and laser treatment. Destruction of MDA-MD-468 cells via pseudo-spherical morphology, detachment, and loss of cell extensions was observed after laser-stimulated AgNP treatment compared to untreated MDA-MD-468 cells.

Based on calculations from Figure 3II–III, the cytotoxic index (IC_{50}) of AgNP-treated MDA-MB-468 cells without laser treatment was observed to be 7.82% and 3.91% with laser treatment after a 72-h incubation. Moreover, MDA-MD-468 cells treated with AgNPs and stimulated by laser treatment were double-stained with calcein-AM/propidium iodide (PI). The stained control MDA-MD-468 cells (non-treated and laser-treated AgNPs) (Figure 3i), AgNP-treated MDA-MD-468 cells (Figure 3ii), and AgNP-treated laser-stimulated MDA-MD-468 cells (Figure 3iii) were observed under an inverted fluorescent microscope to distinguish between dead and alive cells. Uniform green fluorescence (excitation/emission, 495 nm/515 nm) due to polyanionic calcein binding with double-stranded

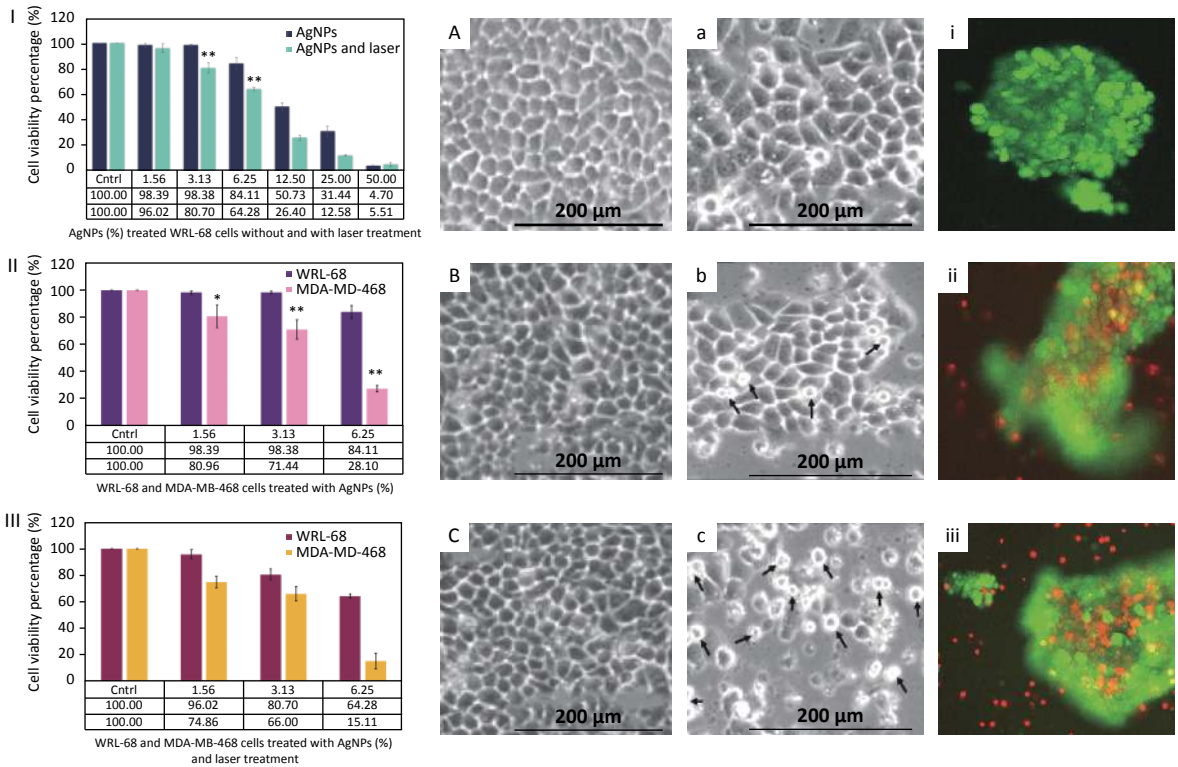

Figure 3. Cell viability percentage of (I) Ag nanoparticle (NP)-treated WRL-68 cells without and with laser treatment, (II) AgNP-treated WRL-68 cells and MDA-MD-468 cells without laser treatment, and (III) AgNP-treated WRL-68 cells and MDA-MD-468 cells with laser treatment. Optical micrographs of WRL-68 and MDA-MD-468 cells (A, a) in non-treated conditions, (B, b) in treated conditions with AgNPs, and (C, c) with AgNPs and laser treatment. Fluorescent images of MDA-MD-468 (i) control cells (untreated), (ii) AgNP-treated cells, and (iii) AgNP-treated cells after laser treatment. $^{*}P < 0.05$, $^{**}P < 0.01$.

DNA in living cells was observed (Figure 3i). Surviving cells were intact with DNA and green nuclei due to the fragmentation of early apoptotic cells. Late apoptotic and necrotic cell DNA was fragmented and stained red. Some red color is observed in Figure 3ii. Conversely, Figure 3iii) shows red color (cell death) due to the destruction of breast cancer cells after the addition of AgNPs and laser treatment. PI penetrates cells with damaged membranes and binds to single-stranded DNA, leading to bright red fluorescence (excitation/emission, 530 nm/635 nm) in dead cells (Figure 3ii–iii).

Spherical AgNPs (12 nm) were synthesized by the PLAL technique. Breast cancer cells were treated with 1.56%–6.25% concentrated AgNPs and stimulated by a 532-nm Q-switched Nd:YAG pulsed laser. The cell viability decreased more dramatically after laser treatment (from 74.86% to 15.11%) compared to without laser treatment (from 80.96% to 28.10%). Therefore, it can be concluded that laser-stimulated AgNPs have the potential to be good photothermal agents that can destroy breast cancer cells by hyperthermic effects without encouraging them to revert to normal slender morphology. The novelty of this research was observed by the reduction in cell viability of breast cancer cells and cell morphology changes after treatment with AgNPs and stimulation by 0.52 J/mm^2 of a Q-switched Nd:YAG pulsed laser at 532 nm.

Disclosures The authors declare that they have no conflict of interest.

Acknowledgement We also thank Mybrain15 MyPhD as a scholarship sponsor for the first author.

[#]Correspondence should be addressed to ISLAM Shumaila, E-mail: shumilesheikh@gmail.com, Tel: 60113 3376187.

Biographical note of the first author: WAN MOHD SHUKRI Wan Norsyuhada, female, PhD, majoring in treatment of breast cancer.

Received: July 8, 2020;
Accepted: January 7, 2021

REFERENCES

1. El-Sayed IH, Huang XH, El-Sayed MA. Selective laser photo-thermal therapy of epithelial carcinoma using anti-EGFR antibody conjugated gold nanoparticles. Cancer Lett, 2006; 239, 129–35.
2. Boca SC, Potara M, Gabudean AM, et al. Chitosan-coated triangular silver nanoparticles as a novel class of biocompatible, highly effective photothermal transducers for *in vitro* cancer cell therapy. Cancer Lett, 2011; 311, 131–40.
3. Yang C, Ma L, Zou XJ, et al. Surface plasmon-enhanced Ag/CuS nanocomposites for cancer treatment. Cancer Nanotechnol, 2013; 4, 81–9.
4. Norsyuhada W, Shukri WN, Bakhtiar H, et al. Synthesis and characterization of gold-silver nanoparticles in deionized water by pulsed laser ablation (PLAL) technique at different laser parameter. Int J Nanosci, 2019; 18, 1850015.
5. Shah A, Latif-ur-Rahman, Qureshi R, et al. Synthesis, characterization and applications of bimetallic (Au-Ag, Au-Pt, Au-Ru) alloy nanoparticles. Rev Adv Mater Sci, 2012; 30, 133–49.
6. Król-Gracz A, Michalak E, Nowak PM, et al. Photo-induced chemical reduction of silver bromide to silver nanoparticles. Cent Eur J Chem, 2011; 9, 982–9.
7. Sulaiman GM, Hussien HT, Saleem MMNM. Biosynthesis of silver nanoparticles synthesized by *Aspergillus flavus* and their antioxidant, antimicrobial and cytotoxicity properties. Bull Mater Sci, 2015; 38, 639–44.
8. Sinha T, Ahmaruzzaman M. Indigenous north eastern India fern mediated fabrication of spherical silver and anisotropic gold nano structured materials and their efficacy for the abatement of perilous organic compounds from waste water-a green approach. RSC Adv, 2016; 6, 21076–89.
9. Varadavenkatesan T, Vinayagam R, Selvaraj R. Structural characterization of silver nanoparticles phyto-mediated by a plant waste, seed hull of *Vigna mungo* and their biological applications. J Mol Struct, 2017; 1147, 629–35.
10. Zou J, Zhu L, Jiang X, et al. Curcumin increases breast cancer cell sensitivity to cisplatin by decreasing FEN1 expression. Oncotarget, 2018; 9, 11268–78.